



HAL
open science

Extrusion as a novel production method for MOX (UO₂-PuO₂) fuel rods: Rheological and physical characterizations on surrogate pastes

Pierre-François Mougard Camacho, Franck Doreau, Romain Castellani, Arnaud Poulesquen, Rudy Valette

► To cite this version:

Pierre-François Mougard Camacho, Franck Doreau, Romain Castellani, Arnaud Poulesquen, Rudy Valette. Extrusion as a novel production method for MOX (UO₂-PuO₂) fuel rods: Rheological and physical characterizations on surrogate pastes. *Journal of the European Ceramic Society*, 2021, 41 (7), pp.4381-4390. 10.1016/j.jeurceramsoc.2021.01.031 . hal-03432397

HAL Id: hal-03432397

<https://minesparis-psl.hal.science/hal-03432397>

Submitted on 24 Apr 2023

HAL is a multi-disciplinary open access archive for the deposit and dissemination of scientific research documents, whether they are published or not. The documents may come from teaching and research institutions in France or abroad, or from public or private research centers.

L'archive ouverte pluridisciplinaire **HAL**, est destinée au dépôt et à la diffusion de documents scientifiques de niveau recherche, publiés ou non, émanant des établissements d'enseignement et de recherche français ou étrangers, des laboratoires publics ou privés.



Distributed under a Creative Commons Attribution - NonCommercial 4.0 International License

Extrusion as a novel production method for MOX (UO₂-PuO₂) fuel rods: rheological and physical characterizations on surrogate pastes

Abstract

To improve the manufacturing efficiency of ceramic MOX fuels, wet processes, such as extrusion, are studied as a novel production method. The flowing behaviour, is essential to obtain smooth and defectless rods. This work provides a study on the rheological properties of the paste and assesses the possibility to produce MOX nuclear fuel by extrusion

Surrogate ceramic powders of UO₂ and PuO₂ were used, respectively TiO₂ and Y₂O₃. A paste with 40.9%_{vol} ceramic loading, yielded smooth, defect free and dense rods. The paste rheology was studied with a ram extruder, using the Benbow-Bridgwater empirical model for ceramic extrusion, and capillary rheometry. The extrusion pressure was predicted using a combination of Benbow-Bridgwater's approach including a Herschel-Bulkley modelling for the extensional flow at the entry die, and for the viscoplastic flow behaviour in the die. The fired extrudates had a homogeneous microstructure and achieved a $95.8 \pm 0.4\%$ density with few micropores.

Keywords

Ceramics, extrusion, rheology, model

1. Introduction

To this day UO₂-PuO₂ MOX fuel has been manufactured via a dry route process [1], [2]. Several of its steps rely on the handling of fine powders (grinding, mixing, sieving and conveyance) prior to uniaxial pressing. In order to limit powder dissemination in the glove box and to improve the mixing of fine particles that tend to agglomerate, new wet routes are investigated.

Extrusion process is one of such alternatives. It tackles the powder dissemination by working with wet ceramic pastes, rather than powders. This process is already used in industry for the production of building materials, bricks, tiles and pipes [3]. In the last decades, the demand for high precision technical ceramics grew, especially in the automotive field for the production of honey-comb like structures [3], [4] such as diesel particulate filters [5], and catalyst carriers [6], [7]. This demand led to several improvements on the comprehension of the process and quality of the produced materials; that is why it can be now considered for a nuclear application. Extruded dense rods can be obtained from pastes with 40-50% powder loading and are robust regarding slight changes on the powders

granulo-morphological properties. These extrudates are smooth, defect free and organic additives can be chosen such as providing proper processability and complete burn-out during debinding and firing steps, therefore, withstanding nuclear fuel requirements.

The goal of this work is to study the feasibility of extrusion process to shape nuclear fuels. It will be assessed in terms of paste rheology, and extrudate physical properties. The pastes need to be formulated so as providing an intended flowing behaviour, namely a desired rheology. Extrudates also need to withstand the physical properties required for nuclear MOX fuels. To the best of our knowledge few studies have been published so far on nuclear fuel extrusion, even less focused on rheology. The most relevant ones concern $\text{UO}_2\text{-ThO}_2$ extrusion [8], [9]. Miller and Liscia were able to extrude 25.4 cm long rods, with satisfactory surface smoothness and achieving more than 93% of the theoretical density, which is the lowest specification for $\text{UO}_2\text{-ThO}_2$ recycled fuel [8]. They formulated a paste containing 0.25%_w of bentonite clay, 0.5%_w of Methocel binder (cellulose derivative), 11%_w of water and 0.25%_w of polyacrylamide as a plasticizer. Their rods showed a high reproducibility in terms of dimensions with a $10.96 \text{ mm} \pm 0.127 \text{ mm}$ diameter and a little deflection of 0.015 cm per 6.72 cm long samples [8]. No rheological data or extrusion curves were provided in this article. Onofrei was also able to extrude UO_2 , ThO_2 pastes obtained from sol-gel processes, with a U/Th content of 0.03. Pastes containing 0.4 to 1%_w of phenolic resin as a binder, and 15 to 24%_w of water were successfully extruded, with 97% of the theoretical density after firing. Again no rheological data were provided [9]. Both papers concluded that extrusion is a viable process to produce high density fuels, with longer aspect ratio than conventional processing methods, smooth surface finish and sufficient reproducibility.

In this study a surrogate ceramic system, $\text{TiO}_2\text{-Y}_2\text{O}_3$ was chosen. Previous studies have shown that they mimic satisfactorily UO_2 and PuO_2 respectively, both in terms of isoelectric neutral point in solution and granulo-morphology [1], [10], [11].

In addition, although ceramic pastes extrusion has been used for years now, at industrial scale the rheological characterizations of the pastes are still based on know-how skills, or on the semi-empiric Benbow-Bridgwater model [3],[12]. In the last decades, academic researchers have added capillary rheometry to the characterization routines as the principle is the same as in ram-extrusion [3], [7], [13] and its physical ground has been widely studied [3], [14], [15], [16]. In the scope of this work, we intend to combine and compare both approaches to help improving the understanding of ceramic paste flows and their limitations. The final goal is to assess the feasibility of extrusion for nuclear fuel production in terms of both physical requirements on the MOX fuel and rheological properties of the paste.

2. Materials & Methods

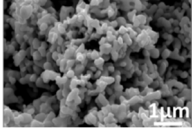
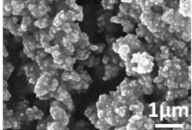
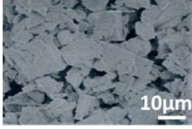
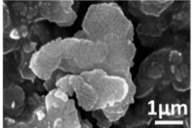
Powder	Supplier	Purity (%)	Particle size (μm)	Particle morphology	Density ($\text{g}\cdot\text{cm}^{-3}$)	Specific surface area ($\text{m}^2\cdot\text{g}^{-1}$)	Isoelectric point in solution (pH)	SEM micrography
UO ₂ (dry route process)	N/A	N/A	0.1 + 0.8	Nanospheres aggregates	10.5	2	5.5 [17],[18]	 [10]
TiO ₂	Marion Technologie	99.9	0.12 + 1	Nanospheres aggregates	3.86	10.1	5.5 [10],[17], [19].	 [10]
PuO ₂	N/A	N/A	1-10	Platelets	11	6	9 [17]	 [10]
Y ₂ O ₃	H.C Starck Grade C	99.95	0.5 + 1-10	Platelets	4.99	14.4	9 [10],[17], [20]	 [10]

Table 1. Physical properties of the surrogates powders TiO₂ and Y₂O₃ and their respective active powders UO₂ and PuO₂

2.1 Raw materials

The TiO₂ powder used in this work is a custom-made anatase titanium dioxide (Marion Technologies, 99.9% purity). It has a median particle size of 0.9 μm (normalized on volume, see Fig. 12 in supporting information). The population is bimodal, as measured by granulometry and depicted on SEM pictures in Table 1. The powder is composed of seemingly hard aggregates of 1 to 10 μm diameter. The subunits are believed to be 120nm nanospheres but do not deagglomerate under such mild conditions (3min mechanical stirring and 30s ultrasonification). The specific BET surface area is 10.1 m^2/g and its pycnometric density 3.86 $\text{g}\cdot\text{cm}^{-3}$.

The Y₂O₃ powder was purchased from H.C. Starck (Grade C, 99.95% purity). It has a median size particle of 1.45 μm . The population is trimodal (Fig. 12) with 0.5 μm , 1 μm and 10 μm diameter plate-like particles (depicted in Table 1). The BET surface specific area was found to be 14.4 m^2/g and the pycnometric density 4.99 $\text{g}\cdot\text{cm}^{-3}$.

As depicted in Table 1 those powders were chosen for their respective granulo-morphological similarities with their respective powders UO₂ and PuO₂. This will be further discussed in section 3.2.

Polyethylene glycol (PEG) with a 400 g/mol molecular weight (Alfa Aesar), was used as both binder and plasticizer [1], [10], [11], [21]. The PEG400 was pure and in a liquid form.

Zusoplast 126/3, a fatty acids mixture with butylglycol as emulsifier (Zschimmer & Schwarz) was used as a lubricant. It was used in liquid form and intended to provide a better compaction as well as non-agglomeration properties by covering the particles with a lubricant layer [21], [23].

Zusoplast C92, a cellulose derivative (Zschimmer&Schwarz), was used as both binder and plasticizer. It was used under powder form [4], [21].

2.2 Devices and techniques

2.2.1 Raw powders characterization equipment

Measurement of specific surface area was carried out in a Micromeritics ASAP 2020 instrument by N₂ adsorption/desorption at 77K according to the BET (Brunauer, Emmett, Teller) method. Prior to measurements, powders were stored overnight at 110°C in a dry desiccator, followed by vacuum degassing operation.

Densities were determined with a Micromeritics AccuPyc II 1340 helium pycnometer.

Morphologies were observed with a Zeiss Supra 55 Scanning Electron Microscope (SEM), equipped with several detectors (EDS and WDS detectors from Oxford Instruments, BSE and SE detectors from Everhart-Thornley and a high resolution SE detector from InLens for high resolutions).

Particle size distribution in water was measured with a Mastersizer 300 laser granulometer from Malvern, using the Mie diffraction theory rather than the Fraunhofer one. Powders ($m < 1g$) were diluted in about 2L of deionized water, mechanically stirred for 3min, and ultra-sonicated for 30s prior to the experiments.

The characteristics of the raw materials are gathered and compared with the UO₂ and PuO₂ data in Table 1.

2.2.2 Pellets and rods characterization devices

The pellets densities were assessed using hydrostatic weighting on a precision scale ($\pm 0.1mg$). Measurements were repeated at least three times on four different samples [24].

Pellets were then dried and cut in half with a wire saw. Pictures were found to have a better quality with the samples observed "as such", rather than prepared in epoxy resin and sputtered with Pt. The SEM used was a Hitachi S4800 FE equipped with a linear detector for back scattered electron X'Celerator (122 punctual aligned detectors).

Other samples from the same rod were crushed in an agate mortar and were characterized in XRD to assess the phases formed during sintering. The XRD device was a Malvern Panalytical X'Pert Pro, with a 1800W generator (45 kV 40 mA measurements settings) using a K α_1 copper anticathode ($\lambda = 1.54056 \text{ \AA}$). XRD patterns were retrieved from a 2θ angle analysis from 5 to 70° with 0.01671° angle steps.

The same samples were then analysed with a TGA to check for the burnout of the polymeric additives. The apparatus was a TGA-DSC, Netzsch STA 409 PC and samples were placed in a 100mL alumina crucible. Measurements were carried out under N₂ at a flow rate of 55mL.min⁻¹ and the temperature was ramped up at 10°C.min⁻¹. Measurements were repeated three times.

2.2.3 Raw materials preparation

Before any paste preparation, the raw materials were stored at 110°C for 24h in a dry desiccator to remove any hygroscopic water absorbed. The TiO₂ and Y₂O₃ were then mixed together with a Braun Hand Mixer 5000WH using the regular kneading blades. The mixing was carried out at maximum speed for 5min. This step was found to be unavoidable due to the small mixing volumes used for each batch, i.e 30 cm³ or 55 cm³ with no possibility of step feeding. With long screw extruders ensuring the mixing, or industrial scales mixing chambers, this step is expected to be unnecessary.

A gel was prepared by mixing the organic additives, i.e Polyethylene glycol 400, Zusoplast C92 and Zusoplast 126/3 with deionized water. The mixture was mechanically stirred at 60 RPM with an IKA Eurostar 20 overhead stirrer during 1h30 and covered with paraffin films to avoid water evaporation. This step ensured the complete dissolution of Zusoplast C92 with the liquid phase.

2.2.4 Paste preparation

Prior to the kneading of the paste in a Brabender's measuring mixer M30/M50, respectively 30 and 55 cm³, it was found necessary to pre-mix the gel and the powder phase to minimize the preparation volume and hence decrease the feeding time in the mixer. Braun Hand Mixer 5000WH was used at 70% speed during 1min30sec to ensure this mixing. A wet powder with an agglomeration tendency was obtained and fed inside the Brabender mixer. This step ensured a proper and repeatable feeding in the mixer chamber.

The feeding was done in two steps, a first addition with around two thirds of the preparation, which quickly formed a paste, and a further addition of the remaining third. Both feeding steps can be seen on Fig. 1, from the beginning to around one and a half minute, and at two minutes respectively. The kneading was carried out at 45 RPM at room temperature during 9min, including the feeding step (2min – 2min30sec). The kneading was considered finished when both the torque and the temperature reached a quasi-steady value. A typical torque value plateau of 8 Nm ± 1 Nm, which is consistent with reported values of 5Nm after 3h mixing for a polymeric-bases ceramic paste [21]. Both 30 cm³ and 55 cm³ mixers were equipped with rollerblade rotors. It was observed that pastes gained 10°C during the kneading, most likely due to particle friction and paste/walls friction. Temperatures differences at the beginning were due to previous kneading that heated the mixing chamber.

The pastes were then recovered and wrapped in paraffin film. The wrapped pastes were stored 24 h at 4°C and 95% ± 3% relative moisture to allow stress relaxation and air bubbles to migrate.

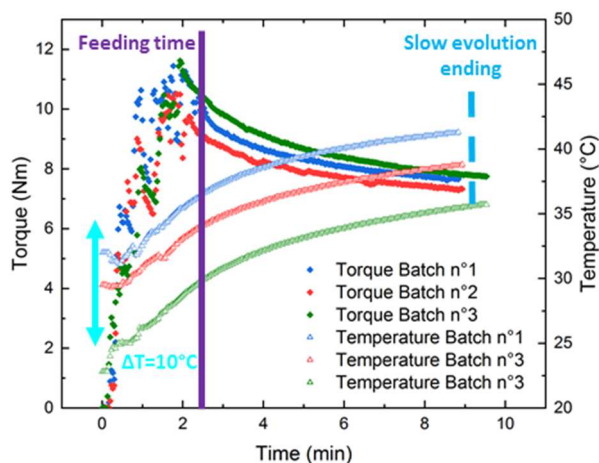


Fig. 1. Typical torque and temperature evolution during the kneading of pastes.

2.2.5 Rheological devices

2.2.5.1 Capillary rheometers

Pastes were tested in a Malvern RH2000 twin bore capillary rheometer. The equipment was used with dies of 0.25 mm and 8 mm lengths, and experiments were carried out with 1 mm, 2 mm and 4 mm diameter dies. For the 0.25 mm long die, aspect ratios (L/D) were 0.25, 0.125 and 0.0625 respectively and for the longer 8 mm die 8, 4 and 2. Dynisco sensors PT422A-70B-6/18 with ranging pressure from 0 to 70 bars were mounted on each bore.

The paste was rolled manually into rods and filled inside the bores. Prior to every experiment a compaction step was performed at a piston speed of 100 mm/min until the pressure reached 0.25 and 0.15 MPa in the bores equipped with the longer and the smaller die respectively. The ram speed was increased gradually to accordingly ramp up the apparent shear rate with five points per decade. Six readings with an 8% pressure deviation were considered necessary before recording the mean pressure value, and automatically ramping up to the next shear rate.

To extend the L/D range, another capillary rheometer (RheoART) manufactured by ARTechnologies was also used. It consisted in a single bore rheometer and was used with several die diameters ranging from 0.93 mm, 1.39 mm, 2 mm and 3 mm with dies aspect ratio (L/D) of 0, 4, 8, 16, and 32. For this apparatus a Dynisco PT422A-70B-6/18 pressure transducer with ranging pressures from 0 to 350 bars was equipped.

A small purge was performed prior to each experiment. After purging 20% of the volume, a 90 sec rest step was performed. Apparent shear rate steps were chosen between 10^{-2} and 10^4 s^{-1} according to the ones accessible with regard to the die diameter and attainable piston speeds. Each step was maintained for at least 10 seconds with a sampling frequency of 4 Hz. Data were checked during post-treatment to assess pressure stability.

Upon the assumptions that the flow is isothermal, that the material is incompressible and that there is no wall slip, data were looked at using a conventional capillary post-treatment data method, described below.

The recorded pressure is actually the total overall pressure; it is therefore needed to isolate the pressure drop corresponding to the flow within the die only. A convenient way to deal with this issue is to use the Bagley correction. It provides a way to determine the pressure contribution at the entrance: using different die lengths with the same diameter, and measuring how the pressure changes with the increasing length, leads to the evaluation of entrance pressures offsets. These pressures are then removed from the data, thus enabling the calculation of the corrected shear stress at the wall using eq.1:

$$\tau = \frac{R}{2L} \Delta P_c \quad (1)$$

where R is the die radius, L its lengths, and ΔP_c the corrected pressure drop [3], [7], [13], [25].

One of the assumptions made to estimate the shear rate at the wall, is that the material exhibits a parabolic velocity profile within the die (Poiseuille flow for Newtonian fluids). As ceramic pastes, or highly concentrated suspensions present non-Newtonian (non-parabolic) velocity profiles, it is then necessary to use the Weissenberg-Rabinowitsch correction to calculate the real shear rate at the wall [7]. The slope of the linear log-log plot of apparent shear rate versus real shear stress provides with the correction needed to determine the real shear rate. The apparent shear rate $\dot{\gamma}_{app}$, defined as:

$$\dot{\gamma}_{app} = \frac{4 \cdot Q_v}{\pi \cdot R^3} \quad (2)$$

is the Newtonian wall shear rate, taken as a reference. Q_v is the volumetric flow, and R the radius of the die. The real shear rate, $\dot{\gamma}_w$, is then calculated from the apparent shear rate and the slope of the apparent shear rate versus corrected shear stress plots (logarithmic values):

$$\dot{\gamma}_w = \dot{\gamma}_{app} \left[\frac{1}{4} \left(3 + \frac{d \ln(\dot{\gamma}_{ap})}{d \ln(\tau_w)} \right) \right] \quad (3)$$

Once the real values of both shear rate and shear stress at the wall are calculated, the viscosities can be determined using eq.4 [3], [13], [25]:

$$\eta = \frac{\tau_w}{\dot{\gamma}_w} \quad (4)$$

Data were also looked at with the Benbow-Bridgwater method detailed in section 2.2.5.2.

2.2.5.2 Extrusion rheometry

Pastes were shaped into cylinders of a diameter similar to the barrel diameter using a hand piston and an external cylinder. These pastes were then fed into the laboratory ram extruder (see Fig.2). This extruder was equipped with different flat dies, with three different lengths 10 mm, 30 mm and 60 mm and having a 10 mm diameter ($L/D=1, 3$ and 6 respectively). The body of the ram extruder was fixed on the bottom part of an Instron 331 electromechanical testing frame, whereas the ram was mounted on the top grip of the 100 kN Instron load cell. No specific displacement captor was used other than the one located in the motor.

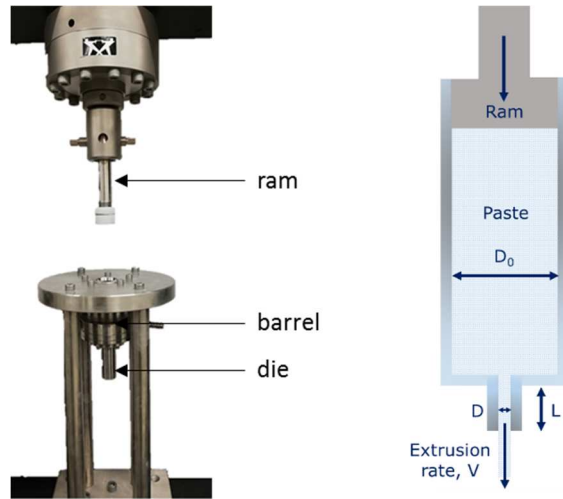


Fig.2. Laboratory ram extruder photography (left) and schematic representation with the conventional notations (right)

Samples were then extruded at constant ram speed V , ranging from 0.1 to 8 mm.s⁻¹, which corresponds to a nine folds extrusion rate. The ram was equipped with a plastic O-ring to avoid material leakage.

Data were treated with two different approaches, the traditional Benbow-Bridgwater method for ceramic extrusion and the capillary extrusion approach as discussed in the previous section.

The Benbow-Bridgwater method relies on decomposing the extrusion pressure into two pressure differences. The entrance pressure due to the constriction of the paste from the barrel to the die entrance, P_e ; and the flowing pressure from die entrance to die exit, P_f . The expressions of both pressures are given by the left and right member of eq.5 respectively, with σ_0 an initial die entry yield stress, τ an initial die-land wall shear stress, m and p velocity exponents and α and β fitting parameters [12], [26], [27], [28]:

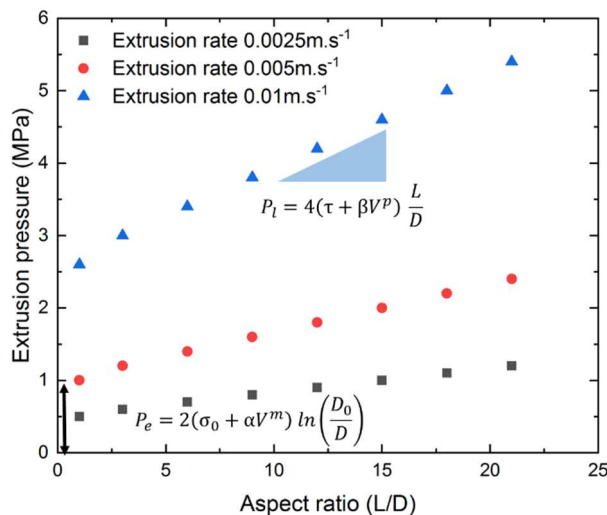


Fig. 3. Benbow-Bridgwater's procedure for the determination of the model parameters (made-up values for easier understanding)

$$\begin{aligned}
P_{ext} &= P_e + P_l \\
&= 2(\sigma_0 + \alpha V^m) \ln\left(\frac{D_0}{D}\right) + 4(\tau + \beta V^p) \frac{L}{D} \quad (5)
\end{aligned}$$

Traditional Bagley plots allow the determination of the parameters σ_0 , α and m by fitting the left member of the equation to y-origins as a function of the extrusion rate. The same methodology is applied to the right member of the equation, which is fitted to the global pressure corrected by the already calculated entry pressures. The methodology is schematized on Fig. 3. One can recall the same methodology as for capillary rheometry, though for the Benbow-Bridgwater model both entry pressure and die pressure are used to characterize the paste [26], [27], [28].

2.2.6 Shaping and sintering

All samples were shaped with the laboratory ram extruder. 20 cm rods were then stored 24 h at room conditions, namely $23^\circ\text{C} \pm 4^\circ\text{C}$ and $60\% \pm 10\%$ relative humidity, to ensure low speed drying. Later the rods were transferred into a 110°C desiccator to enable full drying.

After drying, smaller rods were cut with a wire saw, in order to be able to fit in the debinding and sintering respective ovens. Debinding was performed in a Nabertherm LT9/12 Furnace by heating up the samples from 20 to 900°C at a rate of $0.5^\circ\text{C}\cdot\text{min}^{-1}$ with a 2h30 plateau at 600°C , with no particular atmosphere. The final temperature was chosen such as to provide a pre-sintering as the binder is burned out during the process, and to ensure that the rod develops sufficient strength for the next steps. The sintering was performed in a Nabertherm LHT04/18 furnace by heating the samples from 20°C to 1500°C at a rate of $10^\circ\text{C}\cdot\text{min}^{-1}$ with a 2h plateau at 1500°C under laboratory atmosphere.

3. Results and discussion

3.1 Paste surrogate

Many criteria can be considered when choosing the best surrogates for $\text{UO}_2\text{-PuO}_2$ systems. However, in the scope of this work, the main focus was to study the flowing behaviour of such ceramic paste. Therefore, the main properties to mimic were the ones directly linked to the rheology of the suspensions, i.e morphology and isoelectric point.

As explained earlier, the $\text{TiO}_2\text{-Y}_2\text{O}_3$ is a good candidate to mimic the $\text{UO}_2\text{-PuO}_2$ systems [1], [10], [11]. Indeed, as shown in Table 1, their morphologies are respectively alike, as well as their neutral iso-electric point in solution. It has been shown by authors that high aspect ratio micrometric particles suspensions, present higher viscosities than the same suspension with lower aspect ratio particles, and at the same volumetric loading [29], [30], [31]. Moreover, many authors have also shown that isoelectric point is an important factor dictating the suspension behaviour. When the suspension pH is

close to the particle's isoelectric points, zeta potential values get low and they tend to agglomerate thus increasing suspension viscosity [10], [11], [32], [33], [34], [29]. Therefore, in many applications polymeric dispersants are used to increase this value and obtain a stable suspension [10], [11], [32], [33], [34], [29].

Although densities differ from a factor two to three, it is not believed to play a major role in this study. Pastes are highly charged systems with interaction contacts and the high viscosity of the suspending media should hinder the settling of the particles over the characteristics working times ($1/\dot{\gamma}$). The sedimentation velocity of the particles can be estimated using Stokes' law. Settling speeds of $8.7 \text{ nm}\cdot\text{s}^{-1}$ and $19.7 \text{ nm}\cdot\text{s}^{-1}$ for the surrogate and the active systems respectively were found. Furthermore, when compared to shearing rates of 10 to 10^3 s^{-1} in extrusion processes [21], the settling can be neglected. In addition, pastes formulated and stored up to one month prior to experiments kept showing the same behaviour in extrusion.

The $\text{TiO}_2\text{-Y}_2\text{O}_3$ powder phase referred to this paper, contains 64.49%_w of TiO_2 and 35.01%_w of Y_2O_3 . It was chosen to keep a pertinent volumetric representation of a $\text{UO}_2\text{-PuO}_2$ (70/30 %_{at}) mixture, one of the MOX mixes considered for generation IV fast neutron reactors. This volumetric similarity is important to mimic as both powders differ in morphology. Their volumetric characteristics will thus affect the paste rheology [29], [30], [31].

3.2 Extrusion feasibility and know-how

Defects in extrusion such as delamination upon exiting the die, or liquid phase migration were present in a large extent at first. Liquid phase migration can be evidenced when checking the extrusion pressure signal. Indeed, at constant speed extrusion, the pressure should be stable; an increase over time would give a hint of liquid phase migration within the barrel or the die [35], [36], [37]. The extrudate should also be defectless and smooth. Improper formulation, leads to delamination or breakage of the extrudate [21], [37]. One common and quick testing, used in the ceramic industry to check the proper formulation of the paste, is to make a small filament with the paste and wrap it twice on a finger. If the paste is suitable for extrusion, it should not crack.

Delamination can be caused by multiple factors, such as too low water content, too few additives or in the case of continuous extrusion, shear banding which occurs in the screw nearest area. Such a defect can then propagate to the end of the barrel and even inside the extrudate, causing severe delamination upon drying [21]. A formulation presenting liquid phase migration and its resulting delaminated extrudate is evidenced in Fig. 4. These defects can be dealt with by adjusting the water and plasticizer contents. A too high water content will keep the extrudate from withstanding enough efforts before the firing step. A too low water content will cause delamination during the drying and higher extrusion pressure. Furthermore, pastes with too high extrusion pressure, will present liquid phase migration effects. The pressure gradient will lead to a higher velocity of the fluid within the granular ceramic skeleton, hence driving the liquid phase migration. Polymeric additives, such as plasticizers, increase the relative viscosity of the fluid, hence hindering liquid phase migration. Their burnout is especially relevant in the case of nuclear fuels where reducing atmospheres are used for the

firing step, so that UO_2 does not oxidize to U_3O_8 causing volume changes [8], [9]. Ceramic paste formulation thus requires an equilibrium between polymeric additives contents, water content and ceramic content to be able to yield the desired end-product [4], [21], [38], [39].

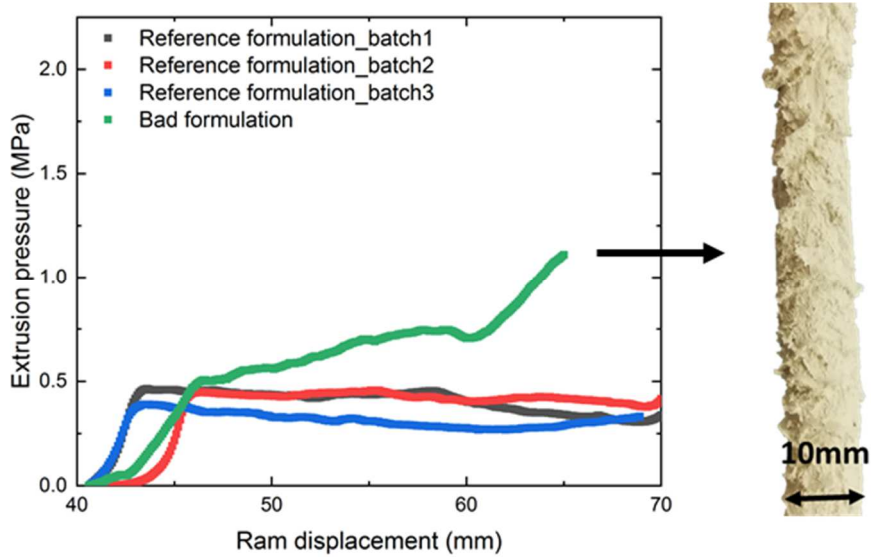


Fig. 4. Liquid phase migration evidence upon extrusion on the left and resulting delaminated extrudate on the right

A satisfactory formulation was found with a gel-phase containing 5.10%_{ow,c} of Polyethylene glycol 400, 2.55%_{ow,c} of Zusoplast C92, 2.82%_{ow,c} of Zusoplast 126/3 and deionized water; % are expressed as weight percentage of the total ceramic weight. The amount of water was chosen so that to have the same volumetric percentage of water and powder in the paste, *i.e.* 40.9%_v water and 40.9%_v powder with 18.2%_v of organic additives (given as volumetric percentages).

3.3 Paste rheology

The main objectives in using rheometry are to extract local intrinsic paste parameters and to use them to predict the global behaviour of the paste, namely the extrusion pressure. Parameters needed for the prediction were estimated piecewise, firstly within the die and then at the die entrance, to provide with a combined model to describe the experimental data. This approach was then compared to the Benbow-Bridgwater' model, which is widely used for ceramic extrusion. The latter is not based on local parameters but rather on a global interpretation of the pressure contributions at the die entrance and within the die.

3.3.1 Capillary rheometry

The experimental data obtained from laboratory ram extruder and two different capillary rheometers have been plotted together in Fig. 5 . Although different equipment with several aspect ratio dies were used, all data align on a single master curve.

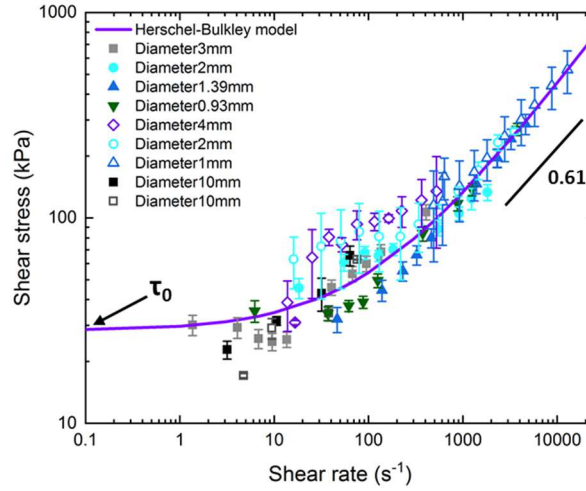


Fig. 5. Shear stresses as a function of the shear rate. The shear stresses were calculated from all extrusion and capillary data. The purple line corresponds to the Herschel-Bulkley model used to describe the experimental data.

In addition, the Herschel-Bulkley model, given in eq.6:

$$\tau = \tau_0 + K\dot{\gamma}^n \quad (6)$$

successfully predicts shear stresses at both low and high shear rates with a consistency, K , of 1.59 $\text{kPa}\cdot\text{s}^{-n}$, a shear yield stress, τ_0 of 28.1 kPa and a pseudo-plasticity exponent, n , of 0.61. This exponent, lower than one, indicates a shear-thinning paste behaviour. On the opposite, shear-thickening pastes would generate high pressures at high extrusion rates, which in turn could lead to liquid phase migration [21]. Shear-thinning ceramic pastes are therefore preferred for extrusion and are usually encountered in the literature [21], [35], [36], [37].

The formulated paste shows also a relative high upstream yield stress (τ_0), which is directly linked to its plastic yield stress by a factor $\sqrt{3}$, according to the Von Mises perfect plastic criterion [40]. Assuming perfect plastic behaviour at low shear rates (typically below 10 s^{-1}), we obtained a plastic yield stress σ_0 equal to 48.7 kPa. The high value of the shear yield stress when compared to the consistency shows that at low shear rates the pastes will behave as an almost perfect plastic material, whereas at medium and high shear rates (typically beyond 100 s^{-1}) the contribution of shearing will be significant, as suggested by the consistency value of $1.59 \text{ kPa}\cdot\text{s}^{-n}$. The values are consistent with ceramic pastes studies in capillary rheometry with shear yield stress between 10kPa and 100kPa, consistencies between $1 \text{ kPa}\cdot\text{s}^{-n}$ and $10 \text{ kPa}\cdot\text{s}^{-n}$ and pseudo-plasticity exponents between 0.3 and 0.65 [7], [38], [41], [42].

The shear rheology of the paste is well described with the Herschel-Bulkley model and can provide a prediction of the pressures developed inside the die. However, due to Bagley corrections, the entry pressures cannot be reverse engineered, except using numerical simulations [43], [44].

3.3.2 Extrusion pressure prediction

In section 3.3.1 we have seen that we were able to correctly interpret the flow within the die, independently of the die geometry with a Herschel-Bulkley model. However, it does not predict the die entrance pressure. For this purpose several options are available. One would be to use Benbow-Bridgwater's model, explained in section 2.2.5.2., where the entrance pressure is predicted using eq.7.

$$P_e = 2(\sigma_0 + \alpha V^m) \ln\left(\frac{D_0}{D}\right) \quad (7)$$

Despite being widely used for ceramic extrusion, and as discussed by several authors [14], [45], [46], Benbow-Bridgwater's model is not based on local parameters and is empirically derived from experimental data. Still it provides with an useful tool to predict extrusion pressures. Another approach was given by Adams and Basterfield for orifice extrusion [46]. In this setup there is no die, so that the total extrusion pressure arises from the cross-section area reduction from the barrel with a diameter D_0 , to the orifice, which can be seen as a 0 mm long die with a diameter D . To describe their data, they used a Herschel-Bulkley model adapted to die entrance geometry (see supporting information). We will refer to this model as a Herschel-Bulkley elongational model, as opposed to the shearing Herschel-Bulkley model from section 3.3.1. for the flow within the die. The model they developed has since be used by author authors for orifice extrusion [47], and also in combination with the same Herschel-Bulkley model that we used for the shearing flow within the die in section 3.3.1 [48].

The entrance pressure is difficult to describe with local parameters as they have proven to be hard to be determined separately, and the pressure drop from the reduction in cross-section area is still described either by using Benbow-Bridgwater's model or the above mentioned Herschel-Bulkley one [12], [46], [49], [50].

In this paper, we decided to use a combination of the already discussed Herschel-Bulkley elongational and shearing models. Thus, we decompose the total extrusion pressure as the sum of two pressures resulting from the cross-section reduction, and the shearing within the die. For the second one we use the capillary expression for the pressure drop within the die eq.1, but rather than using the shear stress τ as such, we use the Herschel-Bulkley model given in eq.6. This yields eq.8:

$$P_t = \frac{4L}{D} \left(\tau_0 + K \left(\frac{8 \cdot V}{D} \right)^n \right) \quad (8)$$

where L/D is the die aspect ratio, V the extrusion rate in $\text{m}\cdot\text{s}^{-1}$ and the Herschel-Bulkley parameters, n , τ_0 and K determined in section 3.3.1. A third contribution is added by considering the small entrance pressure overestimation due to the position of the pressure transducer. Indeed, as the pressure transducers are not located right at the die entrance, there is a small pressure drop contribution because of the transducer displacement (see supplementary information).

The entry term (see supporting information) is given by eq.9 [47], [49], [46]:

$$P_e = 2\sigma_y \ln\left(\frac{D_0}{D}\right) + A \cdot k \left(\frac{2 \cdot V}{D}\right)^n \left(1 - \left(\frac{D}{D_0}\right)^{3n}\right) \quad (9)$$

were A is a coefficient depending on the angle formed by the paste entering the die, σ_y is the elongational bulk yield stress, k the elongational consistency and n the pseudoplasticity index. It has been shown that pastes undergo bulk slippage (shear bands) close to die entrance, creating static zones around the square corners and easing the flow by creating a cone shape. For ease of calculations the angle formed is usually taken as 45° . The A coefficient can be calculated with eq.10:

$$A = \frac{2}{3 \cdot n} (\sin \theta_{max} (1 + \cos \theta_{max})) \quad (10)$$

where $\theta_{max}=45^\circ$ and n is the pseudoplasticity exponent from the flow within the die. The pressures contribution corresponding to the flow within the die was already computed using parameters from section 3.3.1. and eq.8. The pressure arising from the cross-section area reduction (eq.9) had to be fitted to eq.11:

$$P_{experimental} - P_l = P_e \quad (11)$$

in order to obtain all the local parameters needed for the global extrusion prediction according to our final model:

$$P_{model} = 2\sigma_y \ln\left(\frac{D_0}{D}\right) + A \cdot k \left(\frac{2 \cdot V}{D}\right)^n \left(1 - \left(\frac{D}{D_0}\right)^{3n}\right) + \frac{4L}{D} \left(\tau_0 + K \left(\frac{8 \cdot V}{D}\right)^n\right) + \frac{4L^*}{D_0} \tau_0 \quad (12)$$

Fitted parameters are given in Table 2. The flow index was assumed to be the same in both cases and was taken as 0.61 as determined in section 3.3.1. The elongational bulk yield stress was determined as 118 kPa and the extensional consistency as 23.5 kPa.s⁻ⁿ. The high value of the elongational bulk yield stress suggests an important force needed to deform the paste before entering the die, as well as a strong dependence on the extrusion rate with a relatively high extensional consistency. Authors determined similar values for respective elongational bulk yield stress and shear yield stress with an order magnitude difference between the two, such as in this case (see Table 2), but similar elongational and shearing consistencies values. No direct relations were found between the elongational bulk yield stress and the shear yield stress, nor between consistencies, which is surprising as a relation is expected; however the same authors reported similar trends for the elongational bulk and shear yield stress values [49], [48]. In addition it is common for ceramic pastes to present a bulk yield stress somewhere between 50 kPa and 200 kPa with the Benbow-Bridgwater' model [26], [27], [28]. This approach enables a close prediction of the experimental data, see Fig. 6. Though the modelling is not perfect, especially at low extrusion pressures, which corresponds to larger dies and slower extrusion velocities. Attempts were made to correlate the discrepancies observed with the cross-section reduction ratios or with diameters evolution. However, as reported by Wilson et al. [51], no easy correlations were found and the model was no further modified.

σ_y	k	n	τ_0	K
------------	-----	-----	----------	-----

(kPa)	(kPa.s ⁻ⁿ)	(kPa)	(kPa.s ⁻ⁿ)
118	23.5	0.61	28.1

Table 2. Parameters of the Herschel-bulkley models determined for the extensional entrance flow with and the combination of plug and shearing flow within the die

Although the method of section 3.2.3 yielded satisfactory predictions, further work will be carried out to improve the modelling of such pastes flowing behaviour, and on the understanding of the contributions of plug and shearing flows within the die, through different rheological characterizations such as squeeze flow rheometry.

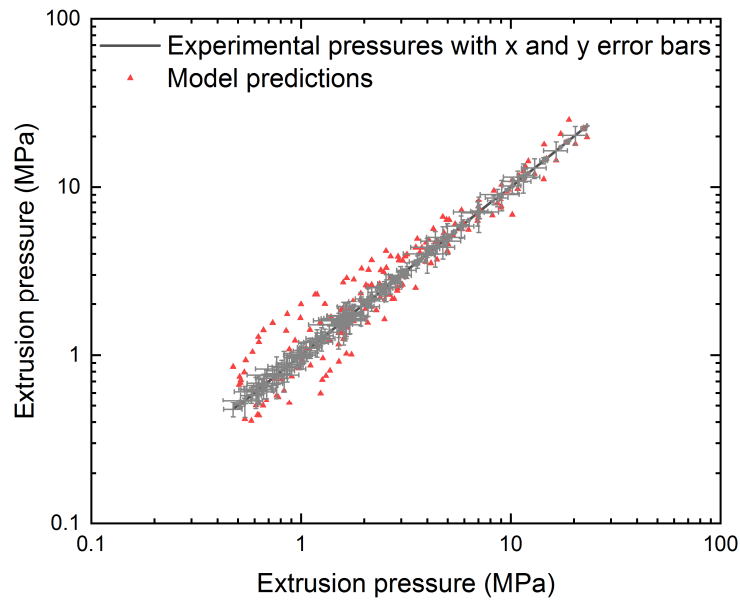


Fig. 6. Log-log plot of the total extrusion pressure as predicted by the model of eq.12 versus experimental pressures plotted with x and y error bars determined as the standard deviation observed experimentally for each of the 187 pressures measured

3.3.3 Benbow-Bridgwater engineering model

To study the rheology of the obtained ceramic paste, the Benbow-Bridgwater model is often used. It provides a global description of the extrusion signal, though its parameters are not local intrinsic material parameters. This model allows to determine a die-entry yield stress of the paste, σ_0 and an initial die-land wall shear stress inside the die, τ . These parameters have to be seen as plastic yield stress and shear stress at the wall respectively, though they lack the physical ground to effectively be the plastic yield stress or the real shear stress at the wall [45], [46], [50].

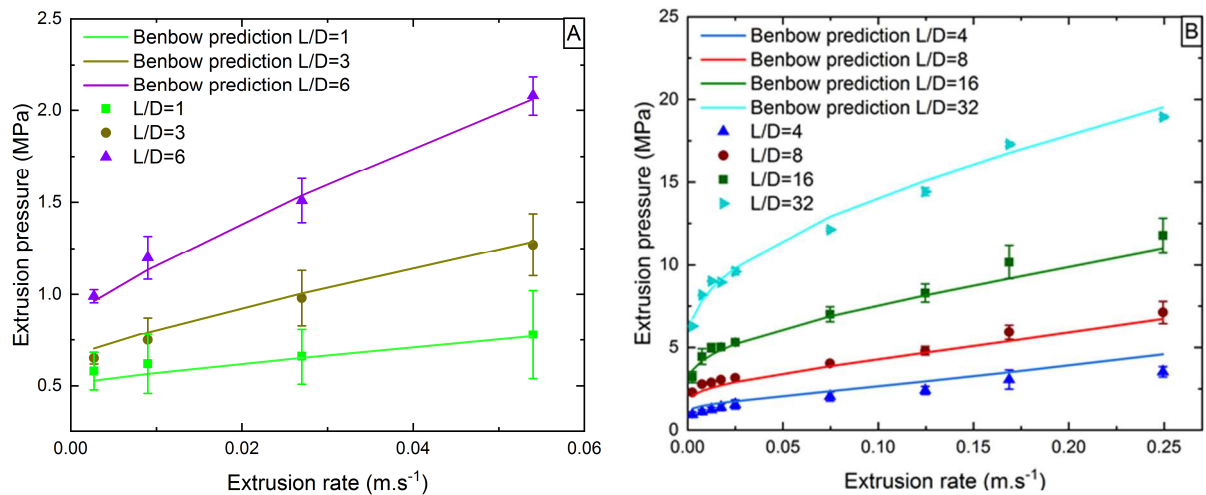


Fig. 7. Extrusion pressures at different extrusion rates obtained with (A) a laboratory ram extruder for different die lengths with 10 mm diameter, purple triangles represent experimental data at L/D=6, lemon green circles at L/D=3 and green squares at L/D=1. (B) a RheoArt capillary rheometer for different die lengths with 2 mm diameter, blue triangles represent experimental data at L/D=4, red circles at L/D=8, green squares at L/D=16, cyan triangle at L/D=32, respective coloured solid lines represent the Benbow-Bridgwater's model predictions which parameters are given in Table 2

The results presented Fig. 7 A and B show an increase of the extrusion pressure with increasing extrusion rates. Significant variations were observed especially at high speeds on the ram extruder when repeating the experiment. Fitting parameters are gathered in Table 2. Variations upon repeating the experiments are less important on Fig. 7 B, suggesting that data are more accurate on smaller diameter dies possibly due to higher shear rates. Plug flow is a characteristic plastic flowing type, encountered in the literature for ceramic paste extrusion. The pressure in such flows shows relative weak dependence upon extrudate velocity, and is directly related to the plastic yield stress of the paste. Thus variations on the paste preparation (small batches) will significantly increase errors upon the determination of the die-entrance yield stress with the Benbow-Bridgwaters approach [51].

The Benbow-Bridgwater model successfully predicts the experimental data (coloured lines in Fig. 7), however, a different set of parameters was determined for each diameter, which could possibly indicate wall slip. Wall slip has not been discussed here, though it has been of interest for many researchers studying the capillary flows of highly concentrated suspensions. It might also help to explain the differences found in the calculated entrance and die consistencies as well as the bulk and shear yield stress differences in section 3.3.2. [7], [13], [52], [53], [54]. Capillary experiments (see section 3.3.1.), and observations, have shown that the ceramic paste obtained is a shear-thinning material. Therefore, values of m and p were restricted to a domain comprised between 0.01 and 0.99. The different parameters found with the Benbow-Bridgwater model, see Table 3, although having the same order of magnitude, shown strong differences when varying the die diameters. Previous researchers had also observed this trend [14], [51]. The initial die-land shear stress has a mean value of $27 \text{ kPa} \pm 26 \text{ kPa}$, and the die-entry yield stress has a mean value of $144 \text{ kPa} \pm 66 \text{ kPa}$. Such incertitude over most relevant parameters represent more than a third of the estimated value. As for fitting parameters α and β , some authors mentioned that a possible interpretation could be carried out

when looking at the terms αV^m and βV^p [4], [39]. αV^m is referred as a “dynamic bulk stress component”, when this term is lower than σ_0 , the entrance pressure mainly arises from the die-entry yield stress. On the contrary higher values suggest a significant contribution of the velocity speed to the entrance pressure. Our data suggest that the entrance pressure was mainly governed by the die-entry yield stress. The βV^p term should be seen as a power-law viscous stress factor. A high value suggests that the extrusion pressure within the die also arises from velocity contributions. On the contrary low values lead to the dominance of the initial die-land wall shear stress and relatively low extrusion pressure increase with the extrusion rate [4], [39]. However, literature agrees that most relevant parameters to look at in the model are σ_0 and τ . Perhaps the other parameters would gain physical meaning if the velocity terms in the equation was also made dependent with dies diameters as suggested by Blackburn [15] and Zheng [16]. Nevertheless, at an industrial scale, this model presents an easy, efficient, and fast characterization for pastes, given a die diameter, especially through the determination of σ_0 and τ [12], [15], [16], [26], [27], [28].

σ_0 (MPa)	α	m	τ (kPa)	β	p	Die diameter (mm)
0.19	2.36	0.99	22	0.49	0.65	0.93
0.07	0.97	0.99	11	0.36	0.60	1.39
0.10	1.35	0.90	39	0.18	0.48	2
0.17	0.70	0.29	0	0.13	0.39	3
0.07	0.45	0.99	61	0.50	0.67	1
0.11	0.30	0.81	66	0.39	0.96	2
0.24	0.90	0.99	0	0.24	0.30	4
0.20	0.61	0.99	18	0.51	0.82	10
0.14	0.96	0.87	27	0.35	0.61	Mean value
0.06	0.65	0.24	26	0.15	0.22	Standard deviation
0.18	0.20	0.99	10	1.92	0.62	Global fitt

Table 3. Benbow-Bridgwater model parameters obtained from fitting each experimental data set separately

To assess the possibility of predicting the extrusion pressures with a unique set of Benbow-Bridgwater model parameters, for any die diameter, a sensitivity analysis was carried out on Fig. 8. For this purpose, a set of mean parameters, determined with the parameters from each die diameter, was used, as well as a set of parameters from a global fit of all data, top of Fig. 8. Finally, standard deviations were added or subtracted from the mean parameter’s values, to determine highest and lower boundaries for the predictions, with σ_0 and τ kept as the mean value, respectively green and purple triangles, bottom of Fig. 8. As can be seen on the top of Fig. 8, the Benbow-Bridgwater model gave more dispersed predictions than the model (red triangles) we used in 3.3.2. Although the global

fit (blue triangles) yielded parameters that led to a better overall prediction than the mean set of parameters retrieved from every die diameter (orange triangles). In addition and as already mentioned, standard deviations on the Benbow-Bridgwater model parameters were significant, and it is noteworthy to say that the model is quite sensitive to those values, as can be seen with the discrepancies between green and purple triangles on the bottom of Fig. 8.

To sum up, this sensitivity analysis showed that although the Benbow-Bridgwater model yields different parameters for every die diameter, a global fit on all data, or considering mean parameters values and providing with uncertainties over some of the model parameters, enables to determine a confident prediction interval for the experimental data for any die diameter/length. At an industrial scale, and already known extruding conditions, it is a reliable model to assess paste properties and compare formulations [14], [21], [51].

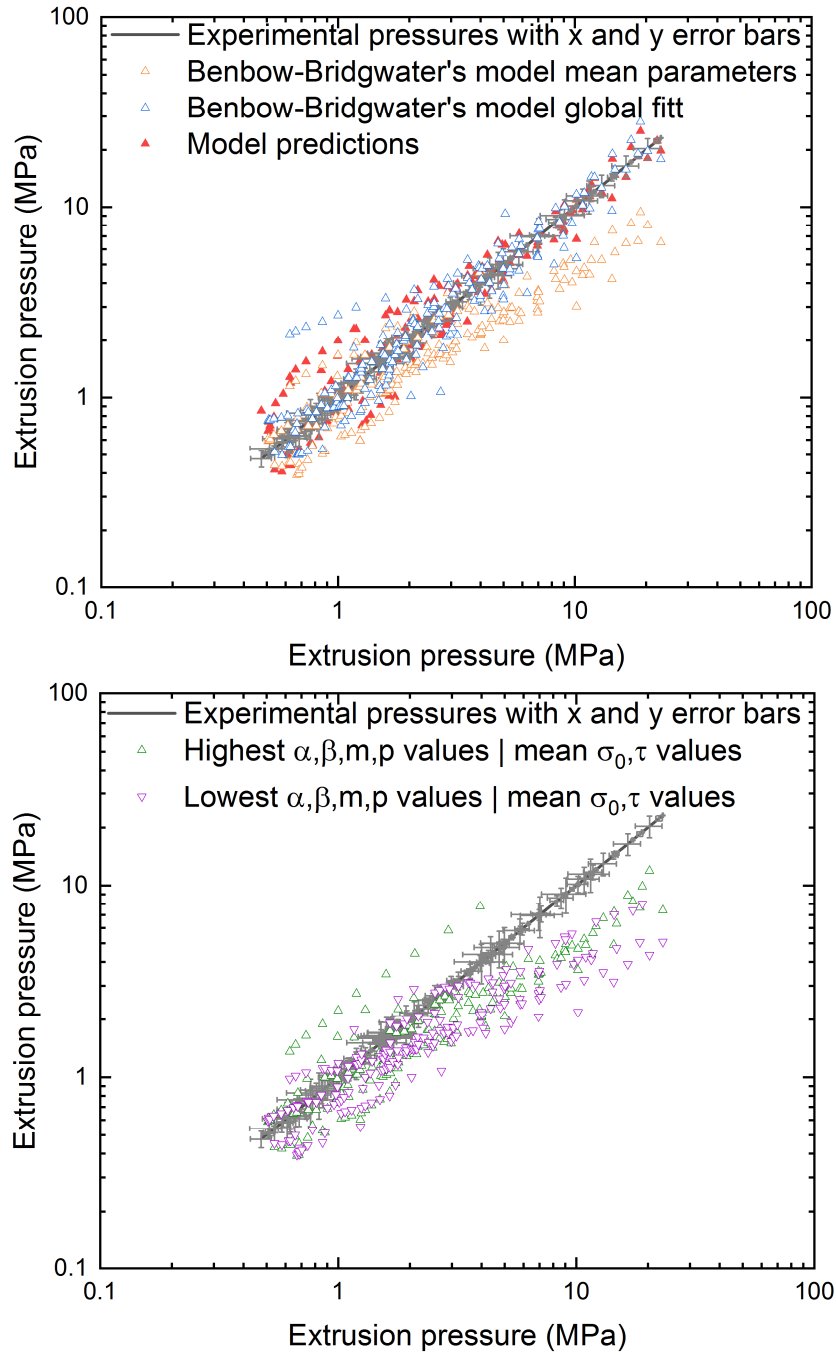


Fig. 8. Log-log plot of the total extrusion pressure as predicted by the Benbow-Bridgwater's model versus experimental pressures plotted with x and y error bars determined as the standard deviation observed experimentally for each of the 187 pressures measured. Orange triangles represent predictions obtained from the mean set of parameters from each die diameter, blue triangles represent the predictions from a set of parameters obtained from a single fitting with all data, and red filled triangles the prediction from the model given in eq.12, whereas green triangles, respectively purple ones, represent the predictions obtained with the mean parameters plus or minus their standard deviation respectively, with σ_0 and τ kept constant

3.4 Extrudate characterizations

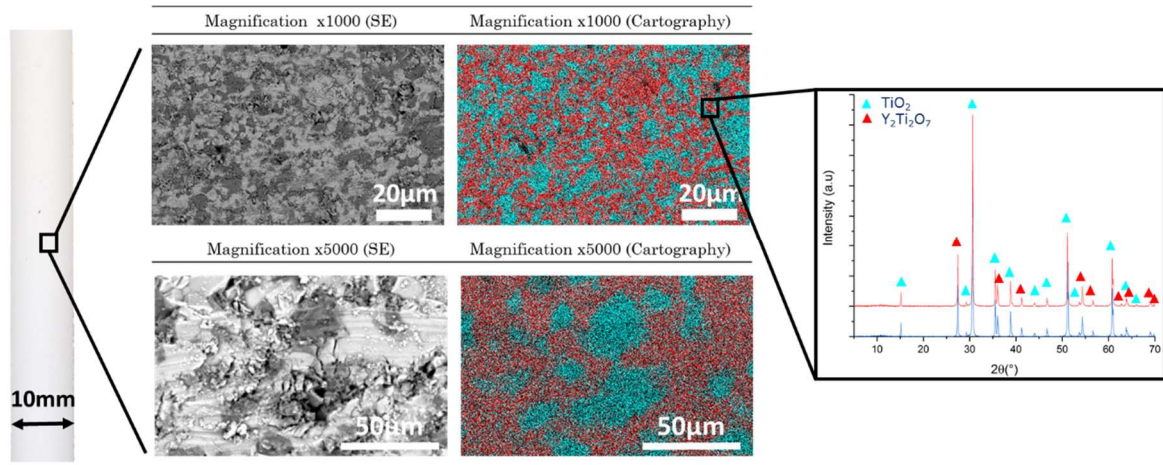


Fig. 9. Pictures of the ceramic materials at different length scale. The photography of the extrudate was taken at the die exit before firing and the SEM pictures and XRD pattern after the firing of the sample

Fired samples extruded at a ram velocity of $1 \text{ mm}\cdot\text{s}^{-1}$ ($9 \text{ mm}\cdot\text{s}^{-1}$ extrusion rate), were further characterized in terms of density, porosity, and chemical composition. A typical rod is presented on the left of Fig. 9. XRD shown the formation of two phases (Fig. 9 right), a pyrochlore phase $\text{Y}_2\text{Ti}_2\text{O}_7$ and TiO_2 rutile, which is consistent with previously reported data [10], [11], and the starting stoichiometry of the mix [55].

Pycnometric measurements on crushed samples gave a $4.63 \pm 0.003 \text{ g}\cdot\text{cm}^{-3}$ density, which is coherent with the value calculated with a mixing law, taking into account the complete reaction of Y_2O_3 to yield $\text{Y}_2\text{Ti}_2\text{O}_7$ and the unreacted rutile TiO_2 .

The relative density of the extrudate after firing was determined with hydrostatic weighting and yielded a $95.0 \pm 0.9\%$ of the theoretical density. This value is encouraging as a minimal 95% relative density is expected for nuclear MOX fuels [1], [11]. TGA measurements on the samples showed no detectable mass variation upon reheating the sample up to 1000°C under nitrogen. These results show the complete burn-out of the polymeric additives during the debinding and firing steps. More thorough characterization will be carried out to determine the exact amount of remaining carbon.

SEM pictures and cartographies taken on the fired extrudates show a satisfactory distribution of both TiO_2 and Y_2O_3 , highlighted in cyan and red respectively (see middle of Fig. 9.) Although TiO_2 forms some clusters, it was expected from the formation of a phase pyrochlore $\text{Y}_2\text{Ti}_2\text{O}_7$ and another TiO_2 rutile [55]. Taking back the topic to radioactive powders, PuO_2 rich clusters in MOx are the ones causing problems and UO_2 should be present everywhere. For surrogates it is then Y_2O_3 that should not form clusters. Although, extrapolating to these conclusions is not so direct. For UO_2 - PuO_2 systems the oxides react to form $(\text{U}_{1-y}\text{Pu}_y)\text{O}_2$ with y supposed to be equal to the chosen molar mixing in the primary mixing step. However, it has been shown that richer PuO_2 phases can form [2]. Which in turn can be a problem for the fuel reprocessing as too rich PuO_2 clusters are much slower do dissolve in nitric acid or even non dissolvable [56]. Richer Y_2O_3 phases (PuO_2 surrogate) could be seen on XRD patterns with a deformation of the $\text{Y}_2\text{Ti}_2\text{O}_7$ peaks [2]. However, no peak deformation were seen on the

XRD pattern, suggesting no formation of other phases than the already mentioned $Y_2Ti_2O_7$ and TiO_2 . This in turn suggests that the mixing was proper and that no Y-richer area are present, which would mean no PuO_2 richer area in the active system. Nevertheless, the pyrochlore phase $Y_2Ti_2O_7$ is well distributed in the sample, which is encouraging for the use of extrusion process to design homogeneous nuclear MOX fuels [1], [10], [11].

4. Conclusions

A satisfactory surrogate ceramic paste of one of the considered MOX UO_2 - PuO_2 mixtures for Generation IV French nuclear reactors (70/30%_{at}) was designed. This paste was composed of a gel-phase containing 5.10%_{w,c} of Polyethylene glycol 400, 2.55%_{w,c} of Zusoplast C92, 2.82%_{w,c} of Zusoplast 126/3, - %_{w,c} % of total ceramic weight-, and deionized water (40.9%_v), representing 59.1%_v of the total volume and 40.9%_v of powder phase containing 64.49%_w of TiO_2 and 35.01%_w of Y_2O_3 . This paste was able to maintain its shape after extrusion and yielded smooth and defectless extrudates with a $95.0 \pm 0.9\%$ density after firing which is in the range for nuclear MOX fuels [1]. Previous work from La Lumia et al., have shown that studies carried out on the same surrogate system leads to transposable results on the active UO_2 - PuO_2 systems [1], [10], [11], .

SEM micrographs show a homogeneous microstructure distribution as well as few observable micropores (darker areas)

All additives have been burned-out during debinding and firing step. A more thorough characterization will be carried out to finally conclude on whether traces of carbon remained.

Rheological studies with a Benbow-Bridgwater traditional approach for ceramics lead to interesting results, with the restriction of a rather low accuracy determination of the material intrinsic plastic yield stress. On the opposite side, the classical capillary rheometry approach, and the use of the Herschel-Bulkley model allowed to obtain more reliable material parameters for the flow within the die. Indeed, it fully characterizes the material over a wide range of shearing rates, i.e. 10^{-2} to 10^4 s^{-1} with three parameters independently of the geometries used. The Herschel-Bulkley model gave a shear yield stress of 28.1 kPa, a consistency of 1.59 $kPa \cdot s^{-n}$ and a pseudoplasticity exponent of 0.61 thus confirming the shear-thinning behaviour observed in extrusion. The Herschel-Bulkley model predicts a plastic behaviour at low shear rates and a viscoplastic one at higher shear rates. Furthermore, the combination of Herschel-Bulkley modelling for the extensional flow at the die entrance yielded a bulk yield stress of 118 kPa with a 23.5 $kPa \cdot s^{-n}$ consistency and the flow index was taken equal as the one in shear, i.e. 0.61. The modelling carried out with the summation of both extensional and shearing flows enable to give satisfactory predictions of the total extrusion pressure.

Future work will focus on more advanced rheological characterizations of the surrogate paste and simulations. It will provide with deeper discussions regarding the rheological experiments and their limitations, with a focus on the development of squeeze flow rheometry for such systems.

5. Acknowledgments

The work was supported by the Commissariat à l'Énergie Atomique (CEA), in partnership with the Centre d'Elaboration et de Mise en Forme des Matériaux (CEMEF – Mines ParisTech). The authors are thankful to Gauthier JOUAN and Mathilde PONS for the SEM pictures taken on the raw powders. The authors would also like to acknowledge their colleagues, Pascal ANTONUCCI, David RUDLOFF, Thomas PIALLAT, Patrice SIGNORET and Marc BATAILLE for their help regarding testing apparatus and material characterizations. A special thanks to Aurélie CHEVALEYRE for the sketches and conception of the laboratory ram extruder used in this project and to Marc CLEMENT for his valuable work on the optimization of extrusion conditions.

6. References

- [1] F. La Lumia *et al.*, « Dense and homogeneous MOX fuel pellets manufactured using the freeze granulation route », *J. Am. Ceram. Soc.*, vol. 103, n° 5, p. 3020-3029, mai 2020, doi: 10.1111/jace.17005.
- [2] S. Vaudez, R. C. Belin, L. Afore, P. Sornay, et S. Grandjean, « A new fabrication route for SFR fuel using (U, Pu)O₂ powder obtained by oxalic co-conversion », *J. Nucl. Mater.*, vol. 442, p. 227-234, 2013.
- [3] W. Gleissle, J. Graczyk, et H. Buggisch, « Rheological Investigation of Suspensions and Ceramic Pastes: Characterization of Extrusion Properties t », p. 13, 1993.
- [4] R. Nath Das, C. D. Madhusoodana, et K. Okada, « Rheological studies on cordierite honeycomb extrusion », *J. Eur. Ceram. Soc.*, vol. 22, n° 16, p. 2893-2900, déc. 2002, doi: 10.1016/S0955-2219(02)00045-6.
- [5] J. Adler, « Ceramic Diesel Particulate Filters », *Int. J. Appl. Ceram. Technol.*, vol. 2, n° 6, p. 429-439, nov. 2005, doi: 10.1111/j.1744-7402.2005.02044.x.
- [6] J. L. Williams, « Monolith structures, materials, properties and uses », *Catal. Today*, p. 7, 2001.
- [7] L. Chevalier, E. Hammond, et A. Poitou, « Extrusion of TiO₂ ceramic powder paste », *J. Mater. Process. Technol.*, vol. 72, n° 2, p. 243-248, déc. 1997, doi: 10.1016/S0924-0136(97)00175-1.
- [8] R. S. Miller et A. Liscia, « Extrusion fabrication of recycled thorium-uranium in the PCUT plant », *Proc. Thorium Fuel Cycle Symp.*, vol. 2, 1962.
- [9] M. Onofrei, « Sol-gel extrusion process for fabrication of (Th,U)O₂ recycle fuel », *J. Nucl. Mater.*, vol. 137, p. 207-211, 1986.
- [10] F. La Lumia, L. Ramond, C. Pagnoux, et G. Bernard-Granger, « Preparation and co-dispersion of TiO₂-Y₂O₃ suspensions through the study of their rheological and electrokinetic properties », *Ceram. Int.*, vol. 45, n° 3, p. 3023-3032, févr. 2019, doi: 10.1016/j.ceramint.2018.10.123.

- [11] F. La Lumia, L. Ramond, C. Pagnoux, et G. Bernard-Granger, « Fabrication of homogenous pellets by freeze granulation of optimized TiO₂-Y₂O₃ suspensions », *J. Eur. Ceram. Soc.*, vol. 39, n° 6, p. 2168-2178, juin 2019, doi: 10.1016/j.jeurceramsoc.2019.01.036.
- [12] J. J. Benbow, E. W. Oxley, et J. Bridgwater, « The extrusion mechanics of pastes : The influence of paste properties on extrusion parameters », *Chem. Eng. Sci.*, vol. 42, n° 9, p. 2151-2162, 1987.
- [13] A. U. Khan, B. J. Briscoe, et P. F. Luckham, « Evaluation of slip in capillary extrusion of ceramic pastes », *J. Eur. Ceram. Soc.*, vol. 21, n° 4, p. 483-491, avr. 2001, doi: 10.1016/S0955-2219(00)00213-2.
- [14] P. J. Martin, « Mechanics of Paste Flow in Radial Screen Extruders », p. 232.
- [15] A. S. Burbidge et S. Blackburn, « A critical assessmet of the Benbow approach to describing the extrusion of higly concentrated particulate suspensions and pastes », *XIIIth Int. Congr. Rheol.*, n° 4, p. 139-141, 2000.
- [16] J. Zheng, W. B. Carlson, et J. S. Reed, « Flow Mechanics on Extrusion through a Square-Entry Die », *J. Am. Ceram. Soc.*, vol. 75, n° 11, p. 3011-3016, nov. 1992, doi: 10.1111/j.1151-2916.1992.tb04380.x.
- [17] M. Kosmulski, « Compilation of PZC and IEP of sparingly soluble metal oxides and hydroxides from literature », *Adv. Colloid Interface Sci.*, vol. 152, p. 14-25, 2009.
- [18] A.-M. Olsson, Y. Jakobsson, et Y. Albinsson, « Surface charges densities of two actinide (IV) oxides : UO₂ and ThO₂ », *Adv. Colloid Interface Sci.*, vol. 70, p. 125-169, 1997.
- [19] R. Greenwood et K. Kendall, « Selection of suitable dispersants for aqueous suspensions of zirconia and titania powders using acoustophoresis », *J. Eur. Ceram. Soc.*, vol. 19, p. 479-488, 1999.
- [20] R. Sprycha, J. Jablonski, et E. Matijevic, « Zeta potential and surface charge of monodispersed colloidal yttrium (iii) oxide and basic carbonate », *J. Colloid Interface Sci.*, vol. 149, p. 561-568, 1992.
- [21] F. Händle, Éd., *Extrusion in Ceramics*. Berlin, Heidelberg: Springer Berlin Heidelberg, 2007.
- [22] J. Gracia, « Étude du comportement du stéarate du zinc en température et sous irradiation - impact sur les propriétés de lubrification », Ecole Nationale Supérieure d'Arts et Métiers, 2017.
- [23] M. Perrault, F. Bertrand, et J. Chaouki, « An investigation of magnesium stearate mixing in a V-blender through gamma-ray detection », *Powder Technol.*, vol. 200, n° 3, p. 234-245, 2010.
- [24] M. Rundans, I. Sperberga, G. Sedmale, et G. Stinkulis, « Effect of sintering process and additives on the properties of cordierite based ceramics », *IOP Conf. Ser. Mater. Sci. Eng.*, vol. 47, 2012.
- [25] B. Lanteri, H. Bulet, A. Poitou, et I. Campion, « Rheological behaviour of a polymer-ceramic blend used for injection moulding », *J. Mater. Sci.*, vol. 31, n° 7, p. 1751-1760, avr. 1996, doi: 10.1007/BF00372188.
- [26] J. J. Benbow, S. Blackburn, et H. Mills, « The effects of liquid-phase rheology on the extrusion behaviour of paste », p. 7, 1998.

- [27] N. Vitorino, M. J. Ribeiro, J. C. C. Abrantes, J. A. Labrincha, et J. R. Frade, « Extrusion of ceramic pastes: An alternative approach to obtain the Benbow's model parameters », *Ceram. Int.*, vol. 40, n° 9, p. 14543-14547, nov. 2014, doi: 10.1016/j.ceramint.2014.05.145.
- [28] S. Blackburn et D. I. Wilson, « Shaping ceramics by plastic processing », *J. Eur. Ceram. Soc.*, vol. 28, n° 7, p. 1341-1351, janv. 2008, doi: 10.1016/j.jeurceramsoc.2007.12.013.
- [29] M. Larsson, A. Hill, et J. Duffy, « Suspension Stability; Why Particle Size, Zeta Potential and Rheology are Important », *Annu. Trans. Nord. Rheol. Soc.*, vol. 20, p. 6, 2012.
- [30] H. Hafid, G. Ovarlez, F. Toussaint, P. H. Jezequel, et N. Roussel, « Effect of particle morphological parameters on sand grains packing properties and rheology of model mortars », *Cem. Concr. Res.*, vol. 80, p. 44-51, févr. 2016, doi: 10.1016/j.cemconres.2015.11.002.
- [31] E. Gregorová, W. Pabst, et J.-B. Bouchet, « INFLUENCE OF PARTICLE SHAPE ON THE VISCOSITY OF KAOLIN SUSPENSIONS », p. 9.
- [32] N. Mandzy, E. Grulke, et T. Druffel, « Breakage of TiO₂ agglomerates in electrostatically stabilized aqueous dispersions », *Powder Technol.*, vol. 160, n° 2, p. 121-126, déc. 2005, doi: 10.1016/j.powtec.2005.08.020.
- [33] B. P. Singh, R. Menchavez, C. Takai, M. Fuji, et M. Takahashi, « Stability of dispersions of colloidal alumina particles in aqueous suspensions », *J. Colloid Interface Sci.*, vol. 291, n° 1, p. 181-186, nov. 2005, doi: 10.1016/j.jcis.2005.04.091.
- [34] B. Peng, Y. Huang, L. Chai, G. Li, M. Cheng, et X. Zhang, « Influence of polymer dispersants on dispersion stability of nano-TiO₂ aqueous suspension and its application in inner wall latex paint », *J. Cent. South Univ. Technol.*, vol. 14, n° 4, p. 490-495, août 2007, doi: 10.1007/s11771-007-0095-z.
- [35] H. Khelifi, A. Perrot, T. Lecompte, D. Rangeard, et G. Ausias, « Prediction of extrusion load and liquid phase filtration during ram extrusion of high solid volume fraction pastes », *Powder Technol.*, vol. 249, p. 258-268, nov. 2013, doi: 10.1016/j.powtec.2013.08.023.
- [36] M. J. Patel, S. Blackburn, et D. I. Wilson, « Modelling of paste ram extrusion subject to liquid phase migration and wall friction », *Chem. Eng. Sci.*, vol. 172, p. 487-502, nov. 2017, doi: 10.1016/j.ces.2017.07.001.
- [37] A. D. U. S. Amarasinghe et D. I. Wilson, « Interpretation of Paste Extrusion Data », *Chem. Eng. Res. Des.*, vol. 76, n° 1, p. 3-8, janv. 1998, doi: 10.1205/026387698524523.
- [38] A. Sirat, M. Belhadri, N. Boudjenane, et T. Bennama, « Extrusion et visualisation des pâtes d'argile au travers des orifices- Application à la céramique (Extrusion and visualization of clay pulp through orifices-Application to the ceramic) », p. 11, 2016.
- [39] F. Raupp-Pereira, M. J. Ribeiro, A. M. Segadães, et J. A. Labrincha, « Extrusion and property characterisation of waste-based ceramic formulations », *J. Eur. Ceram. Soc.*, vol. 27, n° 5, p. 2333-2340, janv. 2007, doi: 10.1016/j.jeurceramsoc.2006.07.015.
- [40] Z. Toutou, N. Roussel, et C. Lanos, « The squeezing test: a tool to identify firm cement-based material's rheological behaviour and evaluate their extrusion ability », *Cem. Concr. Res.*, vol. 35, n° 10, p. 1891-1899, oct. 2005, doi: 10.1016/j.cemconres.2004.09.007.
- [41] G. Racineux, A. Poitou, et F. Chinesta, « Extrusion de supports de catalyseurs : Le problème de la caractérisation rhéologique des pâtes fortement chargées », p. 14.

- [42] G. Racineux, « Rhéologie des pâtes minérales : cas du mélange TiO₂-HNO₃ destiné à l'extrusion de supports de catalyseurs », Ecole Centrale de Nantes, 1999.
- [43] M. Li, L. Tang, F. Xue, et R. G. Landers, « Numerical Simulation of Ram Extrusion Process for Ceramic Materials », vol. Solid Freeform Fabrication Symposium, p. 2011.
- [44] M. Li, L. Tang, R. G. Landers, et M. C. Leu, « Extrusion Process Modeling for Aqueous-Based Ceramic Pastes—Part 1: Constitutive Model », *J. Manuf. Sci. Eng.*, vol. 135, n° 5, 2013.
- [45] J. Zheng, W. B. Carlson, et J. S. Reed, « Flow mechanics on extrusion through a square-entry die », *J. Am. Ceram. Soc.*, vol. 75, n° 11, p. 3011–3016, 1992.
- [46] R. A. Basterfield, C. J. Lawrence, et M. J. Adams, « On the interpretation of orifice extrusion data for viscoplastic materials », *Chem. Eng. Sci.*, vol. 60, p. 2599-2607, 2005.
- [47] X. Zhou, Z. Li, M. Fan, et H. Chen, « Rheology of semi-solid fresh cement pastes and mortars in orifice extrusion », *Cem. Concr. Compos.*, vol. 37, p. 304-311, mars 2013, doi: 10.1016/j.cemconcomp.2013.01.004.
- [48] J. F. Jr. Wight et J. S. Reed, « Non-aqueous Aluminum Nitride Extrusion: II, Die-Land Flow and Tribology », *J. Am. Ceram. Soc.*, vol. 85, n° 7, p. 1689-1694, 2002.
- [49] J. F. Jr. Wight et J. S. Reed, « Non-aqueous Aluminum Nitride Extrusion: I, Die-Entry Flow Behavior », *J. Am. Ceram. Soc.*, vol. 85, n° 7, p. 1681-1688, 2002.
- [50] P. Coussot, « Yield stress fluid flows : A review of experimental data », *J. Non-Newton. Fluid Mech.*, vol. 211, p. 31-49, 2014.
- [51] A. Cheyne, J. Barnes, et D. I. Wilson, « Extrusion behaviour of cohesive potato starch pastes: I. Rheological characterisation », *J. Food Eng.*, vol. 66, n° 1, p. 1-12, janv. 2005, doi: 10.1016/j.jfoodeng.2004.02.028.
- [52] D. M. Kalyon, « Apparent slip and viscoplasticity of concentrated suspensions », *J. Rheol.*, vol. 49, n° 3, p. 621-640, mai 2005, doi: 10.1122/1.1879043.
- [53] M. Mooney, « Explicit Formulas for Slip and Fluidity », *J. Rheol.*, vol. 2, n° 2, p. 210-222, avr. 1931, doi: 10.1122/1.2116364.
- [54] Y. C. Lam, Z. Y. Wang, X. Chen, et S. C. Joshi, « Wall slip of concentrated suspension melts in capillary flows », *Powder Technol.*, vol. 177, n° 3, p. 162-169, août 2007, doi: 10.1016/j.powtec.2007.03.044.
- [55] W. Gong *et al.*, « Phase equilibria of the TiO₂-Y₂O₃ system », *Calphad*, vol. 33, n° 3, p. 624-627, sept. 2009, doi: 10.1016/j.calphad.2009.06.005.
- [56] K. V. Vrinda Devi et J. P. Panakhal, « Quantification of plutonium heterogeneity in (U, Pu) mixed oxide fuel using Passive Gamma Scanning », *Nucl. Eng. Des.*, vol. 255, p. 132-137, 2013.